3-8-2013

Perception based heterogeneous subsurface scattering for film

Laura Wieme

Perception Based Heterogeneous Subsurface Scattering for Film

by

Laura Wieme

A Master's Thesis Submitted in Partial Fulfillment of the Requirements for the Degree of
Master of Science
in Computer Science

Supervised by

Professor Dr. Joseph Geigel
Department of Computer Science
B. Thomas Golisano College of Information Science
Rochester Institute of Technology
Rochester, New York
March 8th 2013

Approved by:

Dr. Joseph Geigel, Professor
Primary Advisor, Department of Computer Science

Dr. Reynold Bailey, Assistant Professor
Committee Member, Department of Computer Science

Prof. Warren Carithers, Associate Professor
Committee Member, Department of Computer Science

Dedication

This thesis is dedicated to David LaFontaine, for his patience and encouragement while I spent all my time rendering. He knew I could do it all along, even when I thought I couldn't.

I'd also like to thank my dad who has always made my education a priority. He probably wasn't aware of the impact it would make when he bought me my first computer in high school and let me keep it in my room. I promised him it was for educational uses and he believed me and supported my early interest in computer graphics. That first computer opened so many doors for me. Thanks dad, I love you.

Acknowledgments

I would like to thank my thesis advisor, Professor Geigel, for feeding my enthusiasm for computer graphics and always pushing me further. Thank you for challenging me. I'd also like to thank my fellow students from Virtual Theatre and the great group of friends I have from RIT and Silicon Valley. Without their constant pestering and encouragement, I probably would not have finished this thesis.

Abstract

Many real world materials exhibit complex subsurface scattering of light. This internal light interaction creates the perception of translucency for the human visual system. Translucent materials and simulation of the subsurface scattering of light has become an expected necessity for generating warmth and realism in computer generated imagery. The light transport within heterogenous materials, such as marble, has proved challenging to model and render. The current material models available to digital artists have been limited to homogeneous subsurface scattering despite a few publications documenting success at simulating heterogeneous light transport. While the publications successfully simulate this complex phenomenon, the material descriptions have been highly specialized and far from intuitive. By combining the measurable properties of heterogeneous translucent materials with the defining properties of translucency, as perceived by the human visual system, a description of heterogeneous translucent materials that is suitable for artist use in a film production pipeline can be achieved. Development of the material description focuses on integration with the film pipeline, ease of use, and reasonable approximation of heterogeneous translucency based on perception. Methods of material manipulation are explored to determine which properties should be modifiable by artists while maintaining the perception of heterogenous translucency.

List of Symbols

Basic Symbols

x position

$\vec{w}$ direction vector

$\vec{n}$ surface normal vector

Ω domain of volume scattering

$\partial\Omega$ boundary of scattering domain

Radiance Symbols

$L(x, w)$ radiance

$L_d(x, w)$ diffuse radiance

$L_{ri}(x, w)$ reduced intensity radiance

$psi(x)$ radiant fluence

$E(x)$ vector irradiance

Surface Function Symbols

$f_r(x, \vec{w}, \vec{w}')$ BRDF function

$S(x, \vec{w}, x', \vec{w}')$ BSSRDF function

$R(||x - x'||)$ dipole BSSRDF function

η relative index of refraction

$F_r(\eta, \vec{w})$ Fresnel reflection coefficient

$F_t(\eta, \vec{w})$ Fresnel transmission coefficient

$F_{ar}(\eta)$ average Fresnel reflectance

$F_{at}(\eta)$ average Fresnel transmittance

$A(\eta)$ Fresnel factor

Scattering Symbols

$p(x, \vec{w}, \vec{w}')$ phase function

μ 0^{th}moment of $p(x, \vec{w}, \vec{w}')$

$\sigma_a(x)$ absorption coefficient

$\sigma_s(x)$ scattering coefficient

$\sigma_t(x)$ extintion coefficient = $\sigma_s(x) + \sigma_a(x)$

$l(x)$ mean free path = $\frac{1}{\sigma_t(x)}$

$\alpha(x)$ albedo = $\frac{\sigma_s(x)}{\sigma_t(x)}$

$\sigma_{sr}(x)$ reduced scattering coefficient = $(1 - \mu)\sigma_s(x)$

$\sigma_{et}(x)$ effective transport coefficient = $\sqrt{3\sigma_a(x)\sigma_t(x)}$

D diffusion constant

Q volume source distribution

Q_0 0th order source distribution

$\vec{Q}_1$ 1st order source distribution

Contents

List of Figures

Chapter 1

Introduction

Translucent materials, such as Pixar's skin model, have redefined expectations for computer generated films and have added a warmth and realism that are highly appealing to audiences. However, more complex translucent materials cannot be modeled with the subsurface scattering material descriptions currently in use by the industry. Heterogeneous translucent materials require more complicated light transport calculations and therefore have been avoided. Recently, a few papers have surfaced with proposed methods for accurately modeling the complex light interactions within heterogenous translucent surfaces and advancing hardware has allowed efficient rendering of objects with complex light transport. In order to be adopted in the film industry, these descriptions must be adapted for a production environment in which ease of use and the breadth of applicational use take priority.

This work advances heterogenous translucent material models to a wider audience, allowing computer graphics artists to simulate a larger range of surfaces. Previous algorithms have been limited to rendering materials that have been captured by a physical model, while

the documented approach creates a more generalized material description based on perception testing to maintain a reasonable approximation of translucency.

In contrast to previous work on heterogenous material modeling, targeting film and artistic use allows for an emphasis on perceived realism over any statistical accuracy. Humans recognize translucency primarily through a noticeable softness and glow we have come to associate with translucent objects we encounter. This can be explained by the way light enters, scatters, and exits a translucent object differently than objects we view as opaque. With this in mind, what factors contribute to a viewer's perception of transparency? What factors become important with the added complexity of heterogeneously composed translucent objects? Most importantly. how can these factors be exploited to create a flexible material model that is efficient and perceptually believable for an audience?

In 2010, Arbree published his Phd thesis presenting a new approach towards a scalable, generalized model for heterogeneous subsurface scattering [1]. His algorithm was able to produce more general approximations of materials while significantly reducing render times. Using his method as a basis for efficient rendering, perception based cues are used to formulate an easily customizable solution for heterogeneous translucent materials for film.

1.1 Contributions

This work makes the following contributions:

- A flexible model of heterogeneous subsurface scattering suitable for film use
- An evaluation of the human perception of heterogeneous materials

- An evaluation of how a heterogeneous material model can be generalized while maintaining perceptual believability

1.2 Chapter Summary

Chapter 2 summarizes the background knowledge of material rendering necessary to truly understand the concepts this work builds upon. The chapter covers the Random Medium Physical Model, the Volumetric Radiative Transfer Equation, the Diffusion Equation, and the subsurface approximation method of BSSRDFs.

Chapter 3 presents the current approaches to translucent materials in commonly used rendering packages. In particular, Maya's Mental Ray, RenderMan for Maya, PBRT, and feature film approaches are examined to emphasize the need for improved models for heterogeneous translucent materials in film.

Chapter 4 summarizes previous work published in the field of heterogeneous subsurface scattering and the perception of materials.

Chapter 5 details the approach taken to create a generalized model of heterogeneous translucent materials for use in films. It also presents the experimentation done to evaluate the impact of perceptual cues on the visual belief of translucency and how such cues can be leveraged in the material approximation.

Chapter 6 discusses the results of the experiments and how it contributed to the final model.

Chapter 7 summarizes the contributions and outcomes of this work

Chapter 8 provides suggestions for future work in developing heterogeneous translucent

models.

Chapter 2

Background

2.1 Random Medium Physical Model

To model the basic physics of light scattering, most materials can be described by a random medium model. Random mediums are composed of particles of random size and form and the medium is defined by the probability of light interactions. Essentially, a random medium can be defined by the following:

Absorption coefficient $\sigma_a(x)$

The absorption coefficient determines the relative distance light of a certain wavelength is able to penetrate a material before being absorbed. Materials with low absorption coefficients will appear translucent for the specified wavelength.

Scattering coefficient $\sigma_s(x)$

The scattering coefficient represents the expected number of scattering interactions.

Phase Function $p(\vec{w}, \vec{w}')$

The phase function is the probability of light scattering from $\vec{w}$ into $\vec{w}$'. The phase function may vary by position; however, most work, such as the Diffusion Equation, requires

that the phase function be normalized and dependent only on the angle between $\vec{w}$ and $\vec{w}'$ [2].

When combined, these three functions form the primary components of the volume rendering equation [17].

2.2 Volumetric Radiative Transfer Equation

To precisely describe the behavior of light within a random medium, the volumetric radiative transfer equation, or VRTE, was introduced by Ishimaru in 1978 [13]. Using a boundary condition, the VTRE builds a description of incident light from all sources and any emission from within the medium. Three different scattering scenarios are accounted for, in-scattering, absorption or out-scattering, and light emitted in the direction $\vec{w}$ by the source. The scenario is visualized in figure 2.1. The medium is described using the absorption coefficient σ_a, the scattering coefficient σ_s, and the phase function $p(\vec{w}, \vec{w}')$ [17].

The volumetric radiative transfer equation:

$$(\vec{w} \cdot \vec{\nabla})L(x, \vec{w}) = -\sigma_t L(x, \vec{w}) + \sigma_s \int_{4\pi} p(\vec{w}, \vec{w}')L(x, \vec{w}')dw' + Q(x, \vec{w}) \tag{2.1}$$

The extinction coefficient σ_t is calculated by $\sigma_a + \sigma_s$ and the phase function is assumed to be normalized. Jensen then integrates the radiative transfer equation over all directions $\vec{w}$ at point x to gain a better understanding of the behavior of light propagation [17].

$$\vec{\nabla} \cdot \vec{E} = -\sigma_a \phi(x) + Q_0(x) \tag{2.2}$$

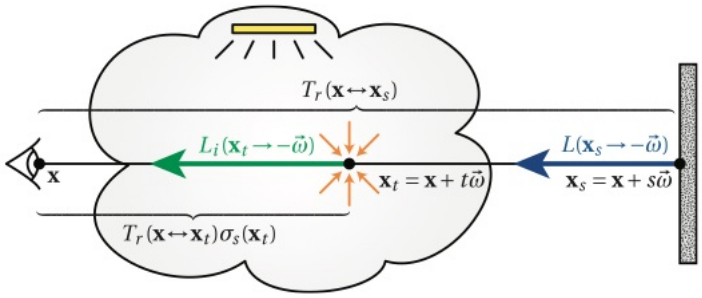

Figure 2.1: Volumetric radiative transfer equation: The final radiance that reaches the viewer ($L(x \rightarrow \vec{w})$) is determined by the sum of the reduced radiance ($L(x_s \rightarrow \vec{w})$) and the in scattered radiance ($L_i(x_t \rightarrow \vec{w})$). [16]

2.3 Diffusion Equation

The diffusion equation is the basis of nearly all current subsurface scattering material models. The diffusion equation makes the assumption that only the lowest order angular dependence of the radiance is needed in a highly scattering medium. Using this assumption, the radiative transfer equation is simplified to a constraint on the fluence at each point. In order to derive the diffusion equation, a diffusion approximation acts as the simplification assumption for the equation.

2.3.1 The Diffusion Approximation

The diffusion approximation is based on the light distribution becoming isotropic in scattering materials. As the number of scattering interactions increases, the light blurs and appears more uniform. First, the radiative transport equation is integrated to relate the scalar irradiance ($\phi(x)$) with the vector irradiance ($\vec{E}(x)$) [17]:

The radiance may be approximated by:

$$L(x, \vec{w}) = \frac{1}{4\pi}\phi(x) + \frac{3}{4\pi}\vec{w} \cdot \vec{E}(x) \tag{2.3}$$

2.3.2 Reduced Intensity Source

When rendering using the diffusion approximation, not all radiance is accurately modeled. Radiance that hasn't scattered yet, usually near a boundary or an interior source, may contain non-linear components that can't be modeled by the simplified assumptions of the diffusion approximation. In order to include this type of radiance, L(x,$\vec{w}$) is separated into L_{ri}(x,$\vec{w}$) for reduced intensity radiance and L_d(x,$\vec{w}$) for the diffusive radiance that can be approximated as shown in figure 2.2. Since the diffusion approximation does not apply to L_{ri}(x,$\vec{w}$), the scattered contribution of L_{ri}(x,$\vec{w}$) is defined by the reduced intensity source:

$$Q_{ri}(x, \vec{w}) = \sigma_s(x) \int_{4\pi} p(\vec{w}, \vec{w}')L_{ri}(x, \vec{w}')d\vec{w}' \tag{2.4}$$

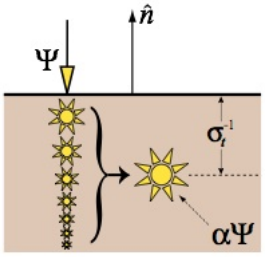

Figure 2.2: Reduced Intensity Source: A beam of light with power Ψ can be approximated by an embedded reduced point source located at one mean free path with a power $a\Psi$ where a is the albedo of the material. [1]

2.3.3 Reaching the Diffusion Equation

A diffusion equation can be built by first substituting the two-term expansion of radiance from 2.3 into the radiative transport equation and integrating over $\vec{w}$:

$$\vec{\nabla}\phi(x) = -3\sigma_t'\vec{E}(x) + \vec{Q}_1(x) \tag{2.5}$$

Where σ_t' is the reduced extinction coefficient formed by the absorption coefficient plus the scattering coefficient multiplied by 1 - the mean cosine of the scattering angle.

And finally by substituting the previous equation into equation 2.2 a classic diffusion equation is reached:

$$D\nabla^2\phi(x) = \sigma_a\phi(x) - Q_0(x) + 3D\vec{\nabla}\cdot\vec{Q}_1(x) \tag{2.6}$$

The diffusion equation can then be solved within the appropriate bounding conditions of the target medium in order to calculate a reasonable approximation of light scattering. Additional details and derivations of the diffusion approximation can be found in [17].

2.4 BSSRDFs

A true simulation of light transport within translucent materials would require solving the radiative transport equation [3], but for homogeneous materials, the effects of scattering can be approximated by a diffusion equation and a scattering term [17]. The resulting bidirectional scattering-surface reflectance distribution function (BSSRDF) is the description of materials that exhibit light transport that enters at one point and may exit at a distant point,

whereas a BRDF assumes that light leaves from the same point it entered. A comparison between a BRDF and a BSSRDF is shown in figure 2.3.

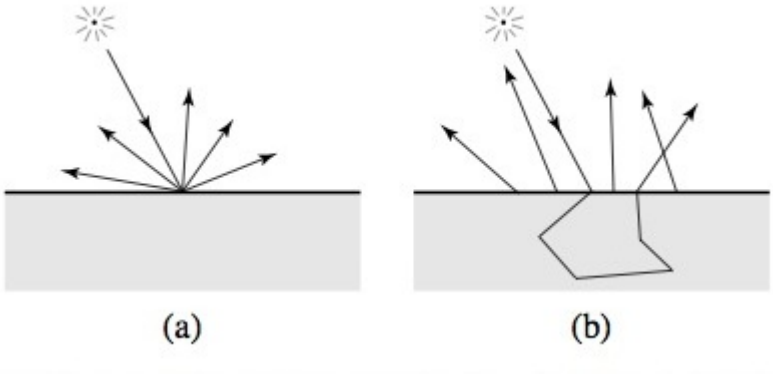

Figure 2.3: Scattering of light in (a) a BRDF, and (b) a BSSRDF. [17].

The BSSRDF is formed by the refractive index of a material, the phase function, and the scattering and absorption coefficients [17]. Scattering and absorption coefficients define the probability that light of a certain wavelength will be scattered or absorbed at a relative distance. The adjustment of these two coefficients can achieve translucent appearances from glass to porcelain and can also impact the perception of scale in generated imagery. The distribution function $S(p_o, \vec{w}_o, p_i, \vec{w}_i)$ forms the ratio of exitant difference radiance of one point (p_o) with the differential irradiance of another (p_i). The BSSRDF then integrates over the surface area and incoming direction in order to form a generalization of the scattering equation in 2.7.

$$L_o(p_o, \vec{w}_o) = \int_A \int_{2\pi} S(p_o, \vec{w}_o, p_i, \vec{w}_i) L_i(p_i, \vec{w}_i) |cos\theta_i| d\vec{w}_i dA. \tag{2.7}$$

The BSSRDF associates the outgoing radiance, L_o at point p_o in direction $\vec{w}_o$ to the incident flux θ_i at point p_i in direction $\vec{w}_i$ [17].

2.5 Summary

Modeling light scattering materials to be realistic is an ongoing problem to balance scientific accuracy with efficiency and artistic control. The scattering approximation formed by a BSSRDF creates an efficient and practical representation of homogeneous subsurface scattering that is visually acceptable. Jensen recognized that previous algorithms oversimplified the local scattering models and therefore produced unconvincing results. His research produced a material model with an exact solution for solving single scattering, combined with a dipole point source diffusion approximation for multiple scattering, that has proven useful for the realistic image synthesis of most general scattering surfaces. In following chapters, a methodology to extend Jensen's scientifically balanced and flexible approach to homogeneous subsurface scattering to heterogenous material rendering will be described.

Chapter 3

Current Approaches to Translucency in Film

Below is an introduction to the subsurface material approaches available in some commonly used graphics packages. Within AutoDesk's Maya, both rendering with Mental Ray and RenderMan will be compared. The renderers were chosen for their proven ability to render homogeneous materials through a generic material preset and the familiarity the material editor provides for a digital artist. Finally, a survey of the current techniques utilized by feature film studios for simulating translucent surfaces is presented.

3.1 Mental Ray for Maya

Mental Ray is a powerful renderer found in Autodesk's commercial graphics packages. Within Maya, there are three Mental Ray materials commonly used for subsurface scattering effects. Example renders from each material are shown in figure 3.1.

3.1a Misss Fast 3.1b Misss Fast Skin 3.1c Misss Physical

Figure 3.1: Translucent material models offered by Mental Ray in Maya

3.1.1 Misss Fast

The popular fast material is appropriate for materials which exhibit shallow light penetration, such as leaves, plastic, and wax. Mi is the prefix used to denote a Mental Ray shader and sss stands for sub surface scattering. It is easily configured and can provide even inexperienced artists with reasonable results with fast and memory efficient render times. The Misss Fast material builds a light map of the surface to store the irradiance data. This provides a model of the diffuse irradiance correlated to the z-depth of the scene which then allows for a fast approximation of a light scattering medium.

Parameters

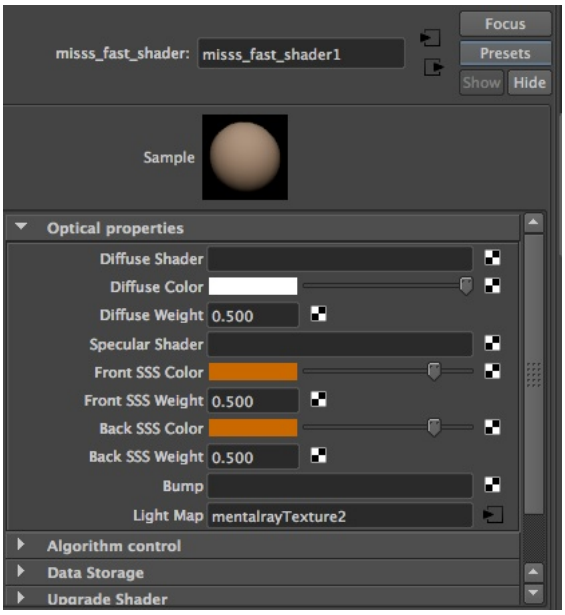

Figure 3.2: Misss Fast Parameters

As shown in figure 3.2, the Misss Fast material is built by compositing a diffuse, specular, and subsurface scattering component. The diffuse shader can take an additional shader to control the diffuse appearance or Maya will default to using Lambert. The diffuse color is applied to all diffuse light, even the scattering contributions. The diffuse weight is just a multiplier for how much of a contribution the diffuse has. The specular shader allows a separate shader to be specified to control specular highlights, but defaults to having no specular. The front and back SSS colors allow separate colors to be specified for the front and through scattered light. The respective weights allow each of these contributions to be adjusted. Bump allows for a bump shader to be assigned to perturb the normals over the surface. The light map is generally auto created to store the front and back surfaces, depth, and irradiant light intensities.

3.1.2 Misss Fast Skin

The fast skin shader is self explanatory. It takes the benefits of the fast material and adds the flexibility of modifying layered surface parameters to simulate the shallow layered scattering effects of skin. It adds a middle scatter layer and some specular color defaults tuned for skin. With the addition of this middle scatter layer it is easy to understand the structure of the model as being constructed from an epidermal, dermal, and subdermal scatter depths.

Parameters

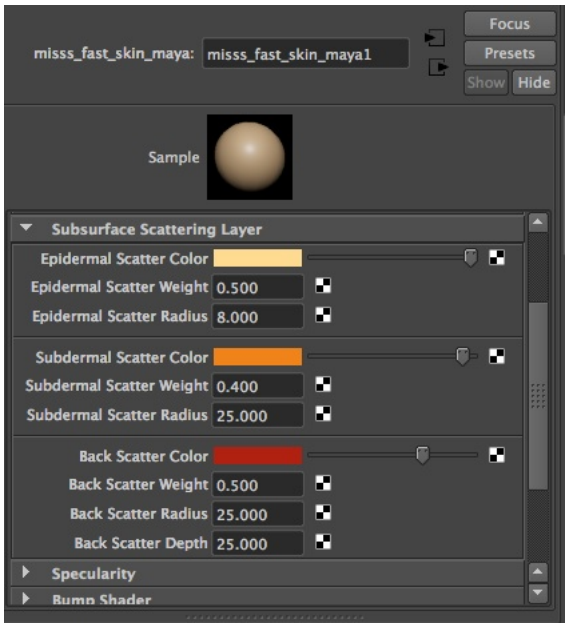

Figure 3.3: Misss Fast Skin Parameters

In figure 3.3, the epidermal scatter color controls the top layer of the skin. By default it is a pale yellow. The epidermal scattering weight determines how much the front scattering is noticeable vs other scattering. The scatter radius defines how deep the scattering effect will go. The subdermal scatter color controls the color of the light scattering below the skin

and also has a weight and a radius. Back scattering is the scattering that happens through the back of the object. This defaults to be red and is most closely recognized with the scattering glow seen on ears. The skin shader then also has a section to specify a separate specular and bump shader.

3.1.3 Misss Physical

The most accurate, yet least intuitive, material provided by Mental Ray is the Misss Physical shader. The material is targeted for accuracy and is recommended for rendering surfaces with deep scattering properties such as milk, blood, soap, and jade. The physical subsurface scattering shader simulates the volumetric scattering of light underneath the object's surface. Photons are stored in kdtree based map. The accuracy of the physical material is due to the simulation of all three types of scattering contributions, diffusion, single scattering, and multiple scattering.

Parameters

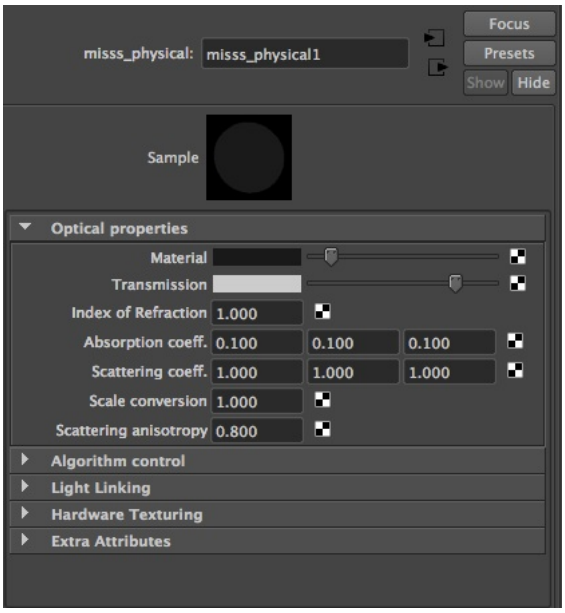

Figure 3.4: Misss Physical Parameters

In figure 3.4, the material parameter allows a shader to be specified to determine the appearance of the material at the surface level. Transmission is a color or texture that determines how the color is filtered as it enters an object. The index of refraction is generally taken from measured index of refractions of physical objects. It describes how light changes direction while entering or leaving an object. The absorption coefficient and scattering coefficient are also taken from empirical data. The scale conversion is used to transform from the world coordinate system to the units used by the scattering and absorption coefficients. The scattering anisotropy determines how uniformly the light scatters, where -1 represents back scatter only and +1 indicates forward scatter only. The value 0 results in uniform scattering in all directions.

3.2 Pixar's RenderMan for Maya

Pixar's RenderMan for Maya adds much of the powerful renderer's functionality into the Maya interface familiar to digital artists. RenderMan's integration into Maya allows a subsurface property to be easily added to any material. Once the material is added to a surface, a separate render pass is also added to generate a brick map that will be used to determine the light scattering depth throughout the model. A sample RenderMan render of a teapot with subsurface scattering can be seen in figure 3.5.

Figure 3.5: Translucent material model offered by RenderMan for Maya

3.2.1 Parameters

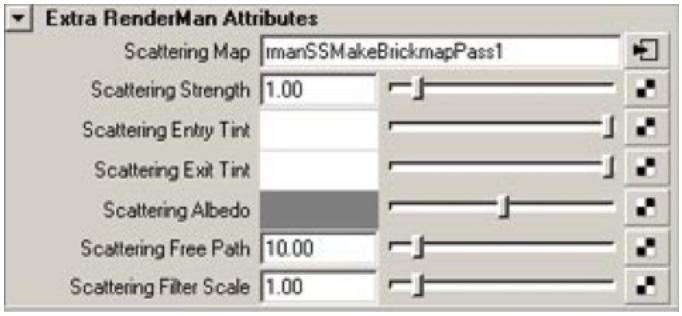

Figure 3.6: RenderMan for Maya Parameters

In figure 3.6, the scattering map gets filled in by RenderMan after computing a scattering pass. This map is also called the brick map. Scattering strength is a scaling value. The scattering entry tint is the color of the light as it enters the object. The scattering exit tint is the color of light as it exits the object. The scattering albedo represents the amount of light reflected from a surface and generally requires a texture map. The scattering free path is the distance the light will travel within the object.

3.3 PBRT

The Physically Based Ray Tracer, or PBRT, is a renderer accompanying the book *Physically Based Rendering* by Matt Pharr and Greg Humphreys. It has become a prime choice for graphic researchers as an easily extendible rendering platform. It is well documented and provides all the fundamentals needed to quickly jump to into advanced rendering algorithms. due to this convention among researchers, this work will focus on the addition of heterogeneous materials within PBRT. From an artist's point of view, PBRT is still fairly technical, but it is far more intuitive than most open source renders and exporters have been written for popular modeling packages.

Subsurface Scattering in PBRT v2 is based on the dipole diffusion algorithm later discussed in 4.1.2. An example render using the dipole based material is shown in figure 3.7.

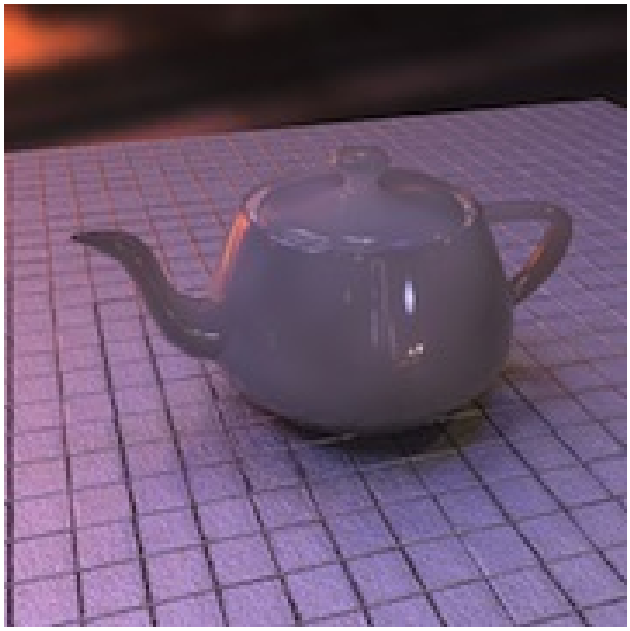

Figure 3.7: Dipole based translucent material offered by PBRT

3.3.1 Parameters

PBRT has two different subsurface materials to chose from with different input parameters. The subsurface material takes a scale value, Kr for a specular texture, sigma a for the absorption coefficient, sigma prime s for the scattering coefficient, eta for the fresnel factor, and then allows for a bump map. The kd subsurface material takes Kd for the diffuse reflection texture, Kr for a specular texture, mfp for the mean free path, eta for the fresnel factor, and then also allows for a bump map.

3.4 Feature Film Techniques

On feature films, subsurface effects are still handled by a technical rendering team. Studios are still developing in house software to try and achieved the most realistic or appealing scattering effects. Most notably, Pixar has continued to improve upon their famous skin material. In the Incredibles, an IIR filter was used to blur sampled data through a voxel grid. Since the stylized look of the Incredibles allowed for a more waxy look, different scatter lengths were used for each color channel, creating pixar's characteristically warm backlit skin. In Ratatouille, improvements were made to the scattering model to capture the realism and improve the artistic control needed for modeling food. Despite the advances in homogeneous translucent material rendering, the problem of heterogeneous material still seems to be avoided. As in the render below, great efforts have been made to simulate light scattering within the cheese, but the lack of heterogeneous subsurface scattering in the marble detracts from the scene.

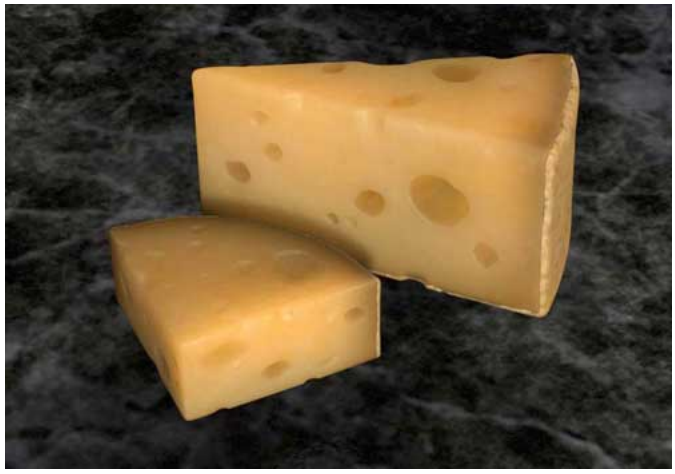

Figure 3.8: Cheese render from Pixar's Ratatouille

Chapter 4

Related Work

4.1 Modeling and Rendering Translucent Surfaces

4.1.1 Monte Carlo Algorithms

Initial algorithms for rendering translucent materials were built upon existing path tracing solutions. Successful rendering of organic layered materials was achieved by Hanrahan and Krueger [12] and Jensen later used the method to simulate the scattering effects of wet surfaces [20]. Despite eventual success, the path-by-path approach used by Monte Carlo algorithms is exceedingly expensive to produce an accurate image. Each path can require the simulation of large numbers of subsurface interactions. Photon mapping reduces some of the cost of basic path tracing by caching paths for later reuse [14]. A map of photon positions and radiances are recorded along the paths from the light sources. Once this map has been generated, it can be referenced for each path from the camera to form the image of the cached radiance data. Photon mapping has been used in film industry rendering solutions, such as Pixar's Photorealistic RenderMan, but rendering subsurface effects for animated scenes using this method requires recalculation of the photon maps and

can result in visual artifacts. An alternative Monte Carlo algorithm, Metropolis sampling [19], improves path tracing efficiency by simulating only the paths deemed to contribute most to the image [19]. The algorithm uses the amount of radiance to mutate its current path and the resulting path is then used to quickly add radiance to the image. Despite advances in path tracing, Monte Carlo Algorithms have been generally inappropriate for film use due to their computational expense.

4.1.2 Dipole Diffusion Algorithms

The primary approach to translucent material modeling is based on the dipole diffusion BSSRDF developed out of the work of Jensen et al. [17] and Jensen and Buhler [14]. For simplification, Ishimaru found that an analytic solution to the Diffusion Equation could be used for infinite, isotropic, and homogeneous materials [14].

$$\phi(x) = \frac{\psi(x)}{4\pi D}\frac{e^{-\sigma_{et}r(x)}}{r(x)} \tag{4.1}$$

ψ is the power of the point light source, r is the distance to the source, and σ_{tr} is the effective transport coefficient.

The dipole method positions two point sources near the surface as a way to satisfy the boundary condition of the diffusion approximation as can be seen in figure 4.1.

Initially, the dipole diffusion BSSRDF was used as a fast alternative to simulating the objects exhibiting subsurface scattering in a path tracer. Later, Jensen and Buhler improved upon the model to reduce calculations down to a two-pass algorithm [14]. The radiance

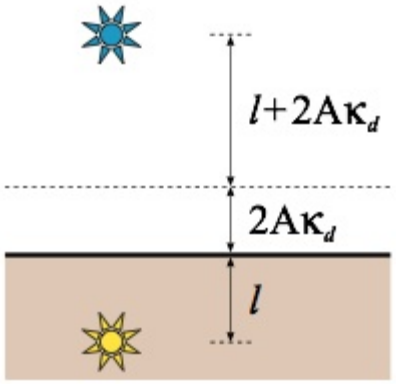

Figure 4.1: An incoming ray is transformed into a dipole source for the diffusion approximation [17].

along the surface is precomputed and the second pass determines the subsurface scattering effects of clusters of similar samples. These improvements make the dipole diffusion BSSRDF very effective for simple scenes, but as Arbree shows, it can quickly become inefficient for large or complex scenes [1].

4.1.3 Heterogeneous Translucent Materials

Heterogeneous translucency builds upon the already complex problem of subsurface light transport to add an additional complication of modeling light interactions within single surface composed of various materials. The majority of current work has been based on simulating a specific measured or synthetic material description and lack generalization and artistic flexibility.

Specialized Algorithms

Most algorithms for heterogeneous materials have been what Arbree calls capture and re-render systems[1]. These systems record models of physical materials, generally photographically, and then utilize the model for simulation in computer generated scenes. The capture process is time consuming and the system is limited to only the scanned material models. Goesele et al. [10] extracted transport coefficients of light within objects and their material from compressed video data. The data is then indexed and used to compute the scattering between regions from arbitrary lighting conditions. Later, Peers followed the same approach, but disassociated the geometry from the material description in order to reuse the material on any object [23]. Tong et al. built upon Jensen's two-pass algorithm to use the dipole diffusion BSSRDF to approximate heterogeneous materials captured from photographs [29]. The captured images are used as textures to control the scattered radiance. Capture and render systems are extremely limited and impractical for film production use where a much more generalized material description would be desirable.

Towards Generalization

Wang et al. [29] approached the problem of creating a generalized heterogeneous material description by using a fast finite difference solution to the heterogeneous diffusion equation. Such an approach was previously implemented by Haber et al. for homogeneous materials [11]. The work by Wang et al. resulted in a real-time system for editing and displaying captured materials applied to arbitrary geometry by warping a material grid. While

possible to achieve reasonable results with this approach, the warping stage is computationally expensive and results may not be accurate without manual adjustment of the material grid.

Recently in his doctoral thesis, Arbree proposes a scalable model for heterogeneous scattering that addresses some of the short comings of previous algorithms by proposing a finite element solution of the heterogeneous diffusion equation [1]. Arbree's algorithm begins by optimizing Jensen et al.'s method [14] by reducing the pre-computation of surface samples to only those points needed for computing the final image. Non-contributing regions include back-facing surfaces and geometry occluded by the camera position. A new diffusion formulation is presented which accurately models the reduced intensity source and the diffusive boundary condition. The Finite Element, or FE, solution to rendering heterogeneous materials has simulated a wide range of materials and complex scenes far more quickly than previous path tracer implementations [1]. Arbree et al.'s work has been the closest to reaching an efficient generalized solution to rendering heterogeneous translucent materials. This thesis will aim for a similar approach with the added assessment of visual cues in a perception based material description.

4.2 Perception of Materials

The human visual system is able to recognize when materials such as soap, milk, and marble are translucent. When presented with computer generated imagery lacking subsurface scattering effects, humans can easily discern translucent objects as fakes. Fleming et al. used a combination of psychophysics and computational image analysis to investigate what

visual cues indicated the appearance of translucent materials [8]. The components studied by Fleming et al. include absorption and scattering coefficients, and lighting conditions.

When presenting observers with a set of images rendered under consistent conditions, all except the presence of specular reflections, people associated glossy surfaces as more translucent [8]. This reaction is credited to the majority of common translucent objects having a specular highlight (e.g. marble, plastic, or leaves) and the assumption that the visual system may then associate and expect translucent materials to appear glossy. It was also shown with this test that the human visual system overlooked inconsistencies between the transmitted light and the resulting reflections. Observers responded that inconsistent images that met their expectations of translucency looked more realistic that the images that were lit to be physically consistent.

The second psychophysical test for translucency studied the impact of light source direction on the perception of translucency. The test consisted of a computer generated image on the left and a similar scene on the right with different fixed lighting conditions. The user was given a perceived opacity slider with the task of adjusting the scene on the right to match the image on the left. The slider adjusted the scattering coefficient through 128 non-linear steps from 0.4 to 60. It was found that changes in lighting direction significantly altered the perception of translucency. Objects lit from behind tend to be perceived as highly translucent, whereas objects lit from the front appear opaque [8]. This is credited to the enhanced appearance of the visual softness and glow that humans interpret as translucency. Particularly, back lighting small, thin areas gives a very clear sense of translucency since it provides a distinct inner glow.

In order to segregate the visual cues that contribute to translucency, changes in image appearance were analyzed as parameters of the BSSRDF were altered. Additional properties explored include color saturation, image contrast, and spatial structure. Since white light through a colored translucent object becomes color, it was first assumed that saturation could have reasonable impact on the perception of translucency. However, Fleming and Bulthoff's work found that saturation could slightly influence the perception of translucency, but it did not provide a significant impact alone [7]. Of more significant visual impact was the presence of bright, blurred fringed along the edges and corners of objects. It is suggested that adding bright edges and appropriate specular highlights could be a reasonable substitute for a full BSSRDF in some use cases. Deemed the most important visual cue in translucency perception by previous work, image contrast was shown to alter translucency when an image's intensity histogram was adjusted [7].

Building upon the previous work done on perceived translucency, it seems possible to create a simplified description of translucent materials that will be better suited to the needs of film production. Additional experiments will be required to determine the visual cues that differentiate the perception of heterogeneous from homogeneous translucent materials.

Chapter 5

Methodology

In this chapter, the approach to creating a generalized heterogeneous translucent model for film is presented, as well is the methodology of perception experiments. The primary goal of the experiments is to examine the human perception of heterogeneous translucent materials and what pieces of the rendering solution can be approximated without a loss of believability.

The focus of the material description formed in this work is to provide an efficient and intuitive description of heterogeneously composed translucent materials suitable for film production use. Due to the nature of its purpose, perceptual realism and creative flexibly are valued over a physically accurate simulation. The results of the material description and perception experiments will be presented in chapter 6.

5.1 Heterogeneous Diffusion

To begin rendering heterogeneous translucent materials using the diffusion equation, a boundary condition and a source model must be chosen to form a diffusive source boundary

condition that will be used to approximate the multiple scattering within the material. The boundary condition is already chosen as the Robin boundary condition has been previously shown to be the most accurate [1]. Two source models are suitable for use as the reduced intensity source in the diffusive source boundary condition. The embedded source model places point sources into the medium and is well suited to approximating homogeneous subsurface scattering, but the boundary source model is better suited to the heterogeneous problem. Since the boundary source model represents the source as the diffuse flux arriving at the boundary and as it is distributed on the surface, less samples are needed to accurately model the features of a heterogeneous material[1].

5.1.1 Diffusive Source Boundary Condition

Using the Robin boundary condition and the boundary source model, the diffusive source boundary condition can be found for use with the diffusion equation to solve for heterogeneous scattering. The condition forms a relationship between the internal inward diffuse flux, internal diffuse flux reflected at the boundary, and the incoming flux refracted from the external sources [1].

$$\Gamma_d^{in}(x) = \Gamma_d^{ref}(x) + \Gamma_s(x) \tag{5.1}$$

$$\Gamma_d^{in}(x) = \int_{(\vec{n}\cdot\vec{w}<0)} L_d(x,\vec{w})(-\vec{n}\cdot\vec{w})d\vec{w} \tag{5.2}$$

$$\Gamma_d^{ref}(x) = F_{dr}(\eta) \int_{(\vec{n}\cdot\vec{w}<0)} L_d(x, -\vec{w})(-\vec{n}\cdot\vec{w})d\vec{w} \tag{5.3}$$

$$\Gamma_s(x) = e^{\frac{\sigma_a(x)}{\sigma_s(x)}} \int_{(\vec{n}\cdot\vec{w}<0)} F_t(\eta, -\vec{w}) L(x, -\vec{w})(\vec{n}\cdot\vec{w})d\vec{w} \tag{5.4}$$

Equation 5.3 scales the internal diffuse flux incident on the boundary by the average Fresnel reflectance coefficient $F_{dr}(\eta)$ to calculate the reflected internal diffuse flux. Equation 5.4 scales the incoming light by the Fresnel transmittance coefficient $F_t(\eta, \vec{w})$ and the approximation of absorption before the light diffuses. This results in the incident external radiance being split into the refracted, internal, and diffuse radiance contributions. To reach the diffusive boundary condition, Equations 5.2 and 5.3 are substituted into the relationship formed by Equation 5.1. The diffusion approximation (Equation 2.3) can then be substituted for $L_d(x, \vec{w})$. The derivation of the resulting equation results in the diffusive source boundary condition (Equation 5.5) needed to solve the heterogeneous scattering problem [1].

$$\phi(x) + 2A(\eta)K_d(x)(\vec{n}\cdot\vec{\nabla})\phi(x) = \frac{4}{F_{dt}(\eta)}\Gamma_s(x) \tag{5.5}$$

The coefficients are carried over from the original Robin boundary condition.

5.2 Finite Element Solution

The Equation 5.5 representing the heterogeneous scattering problem is computationally expensive to solve. One of the largest contributions of Arbree's work was the use of a Finite Element solution to efficiently solve the equation. The efficiency and accuracy of the approximation solutions reached using the Finite Element method also make it an appropriate solution for this work's film-targeted model. Finite Element algorithms solve a partial differential equation searching a fixed space of trial solutions for a function that best approximates the solution. Since the diffusion equation is a second order partial differential equation, a finite element solution can easily be applied. The particular method leveraged for solving the heterogeneous diffusion equation is based of the Lax-Milgram Theorem [1].

Theorem 1. *Lax-Milgram Theorem: Let* $\mathbb{H}$ *be a Hilbert space. Given a bilinear functional* $\mathcal{H} : \mathbb{H}x\mathbb{H} \rightarrow \mathbb{R}$ *that is bounded and coercive, i.e. there exsist constants* $\alpha, \beta > 0$

$$\forall u, v \in \mathbb{H}, |\mathcal{H}[u, v]| \geq \alpha \parallel u \parallel \parallel v \parallel \tag{5.6}$$

$$\forall u \in \mathbb{H}, \beta \parallel u \parallel \geq \mathcal{H}[u, u] \tag{5.7}$$

and a linear function $\mathcal{F} : \mathbb{H} \rightarrow \mathbb{R}$ *there is exactly one function* $v \in \mathbb{H}$ *such that*

$$\forall u \in \mathbb{H}, \mathcal{H}[u, v] = \mathcal{F}[u] \tag{5.8}$$

This theorem can be used to solve the weak form of the partial differential equation. The Lax-Milgram theorem guarantees that a weak solution exists and is unique. The resulting

function is either the solution of the diffusion equation or it is the closest function in $\mathbb{H}$ to the solution. With the diffusion equation and the diffusive source boundary condition, a linear system can be reached that is then solvable by the Finite Element method.

5.3 Diffusion Equation Weak Form

In order to reach a form that can be solved by the Lax-Milgram Theorem, the diffusive boundary condition (Equation 5.5) must be split into its bilinear form and its linear form. Based on the theorem, if $\mathbb{H}$ is an arbitrary space of functions and $\theta \in \mathbb{H}$ can be any function, the linear form can be reached by multiplying Equation 5.5 by θ and integrating over the volume Ω.

$$-\int_{\Omega}[\vec{\nabla}\cdot(K_d\vec{\nabla}\phi(x))]\theta dx+\int_{\Omega}\sigma_a\phi\theta dx=\int_{\Omega}Q^0\theta dx \tag{5.9}$$

The right side of Equation 5.9 is the linear form required by the theorem. The weak form can then be reached with the application of the divergence theorem followed by a simplification using the diffusion source boundary condition.

Theorem 2. *Divergence Theorem: Let v be any vector function and u be any scalar function then:*

$$\int_{\Omega}\vec{\nabla}udx=\int_{\partial\Omega}u(v\cdot\vec{n})dx-\int_{\Omega}u(\vec{\nabla})dx \tag{5.10}$$

The diffusion source boundary condition eliminates the gradient term,$K_d(\vec{n}\cdot\vec{\nabla})\phi$, to create the weak form needed to use Lax-Milgram.

5.4 Weak Form to Linear System

Finally, it is assumed that $\mathbb{H}$ has a finite basis so that the weak form can become a linear system. Given a finite basis, if $n = |B|$ then the following is a system of equations for ϕ[1].

$$\int_{\Omega}[K_d\vec{\nabla}\phi\cdot\vec{\nabla}\beta_i dx] + \int_{\Omega}[\sigma_a\phi\beta_i dx] + \frac{1}{2A}\int_{\Omega}[\phi\beta_i ds] = \int_{\Omega}[Q_0\beta_i dx] + \frac{2}{AF}\int_{\Omega}[\Gamma_s\beta_i ds]\forall\beta_i \in B \tag{5.11}$$

5.5 Implementation

This section describes the approach taken to implement the algorithms previously explained. The implementation builds upon the existing Physically Based Ray Tracer (PBRT) architecture. PBRT is frequently used for rendering research and offers both a direct comparison to previous works and a readily available environment for others to reproduce or continue this work. Building a basis, creating the finite element system, and solving the linear system will be covered. In building a basis in section 5.5.1, a mesh with a simplified basis function is generated. This is the setup to create a sparse matrix suitable for applying the equations found in section 5.2. In section 5.5.2, the resultant tetrahedral mesh from section 5.5.1 is used to compute the Finite Element System described in 5.2. Finally, 5.5.3 solves the the linear system by taking the Finite Element System, reaching it's diffusion equation weak form described in 5.3, converting that result to the linear system described in 5.4 and then solving using a conjugate gradient algorithm with a symmetric successive over-relaxation precondition from libMesh [1] .

5.5.1 Building a Basis

The basis for the finite element matrix is a piecewise-linear basis on a tetrahedral mesh. Tetgen is used to quickly generate tetrahedral meshes from triangle surface geometry such as the mesh shown in figure 5.1. In the tetrahedron, each basis function lies only in one ring, sharing a central support vertex. This limit causes the resulting matrix to be sparse and efficient to solve with the finite element algorithm.

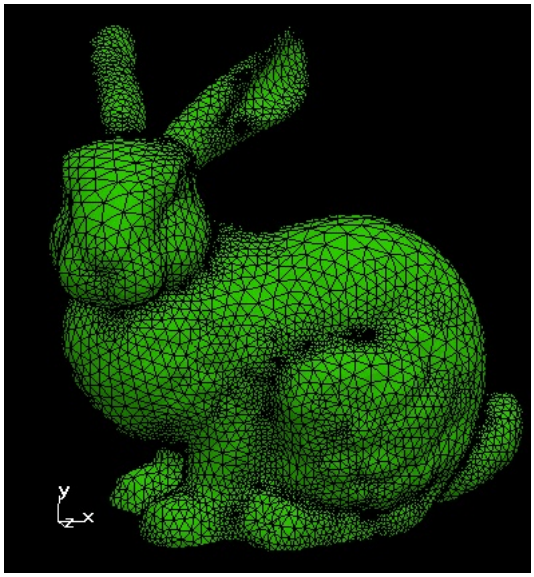

Figure 5.1: Bunny as a tetrahedral mesh

5.5.2 Creating the Finite Element System

Once the mesh is in its tetrahedral form, the equation becomes the sum of the integrals the volumes and faces of the tetrahedra. To create the finite element system, a set of nested loops over tetrahedra, quadrature points, and basis functions compute the sums of the values of the integrand at each quadrature point.

```
SparseMatrix f_mat ;
Vector r_vec;
matrix.zero();  rhs.zero();
foreach Tet t in mesh {
  foreach QuadPt pt in Tet {
    foreach Basis i in Tet {
      foreach Basis j in Tet {
        f_mat[i,j] += pt.wt  Kd(pt)  dot(grad(i,pt),(grad(j,pt)));
        f_mat[i,j] += pt.wt sigA(pt) value(i ,pt) value(j ,pt);
      }
      r_vec[i] += pt.wt src(pt) value(i,pt);
    }
  }
  foreach Face f of Tet {
    if(f on boundary) {
      foreach QuadPt pt on f {
        foreach Basis i in Tet {
          foreach Basis j in Tet {
            f_mat[i,j] += (0.5/A)  pt.wt value(i ,pt) value(j ,pt);
          }
          r_vec[i] += (2/A)  pt.wt gamma(pt) value(i,pt);
        }
      }
    }
  }
}
```

Listing 5.1:]Pseudo-code for the assembly algorithm [1]

5.5.3 Solving the Linear System

A sparse matrix algorithm is used to solve the linear system created by the Finite Element Diffusion Equation. As long as the material coefficients and source functions are bounded and have bounded derivatives, a solution can be found [1]. The pseudo code in listing 5.1 shows how it can be done. By preprocessing the mesh with a tetrahedral basis, the bounds requirement is met. The system is then solved using the conjugate gradient algorithm with a symmetric successive over-relaxation precondition from libMesh [1].

5.5.4 Parameters

Given all the complicated equations required to render heterogenous translucent objects, it is necessary to simplify the user facing parameters to a more intuitive set of controls for artists to achieve the desired visual result. The material description provided in this paper builds off of the approach taken by Jensen and Buhler [18]. Their approach takes a diffuse reflection color, the mean path length, and the index of refraction as parameters to then derive the materials scattering properties. For this approach, the material takes a diffuse reflection texture (Kd), a specular texture (Kr), a scale value for representing the scale of the model, and a mean free path texture for making the material more or less translucent. By making most of the parameters able to use texture input, laying out a material is more intuitive to a visual artist. Since directly setting absorption and reduced scattering coefficients is difficult to visualize and their effects are nonlinear, using the utility function SubsurfaceFromDiffuse() allows us to mathematically reach the required equation components through the inputs that were more user intuitive [24]. More detail on choosing or obtaining plausible material values/textures is covered in section 6.1.2.

5.6 Perception of Heterogeneous Translucent Materials

5.6.1 Approach

The human visual system does not directly interpret physical statistics while processing how translucent an object appears. Measured material values can achieve varied perception

of translucency when image cues such as color, blur, and contrast are adjusted. [Fleming] Building upon the work in "Perceiving translucent materials", a test application was made to test the impact of visual cues on the perception of heterogeneous translucent surfaces. Fleming's approach was appealing as they evaluated perception of a complex 3D object from a single image as opposed to the flat slab tests of the past. The test consisted of a variety of renders produced on a Macbook Pro with at NVIDIA GeForce 9600M GT 512 MB graphics card and presented on the built in LCD display. The images were generated within PBRT using variations on the heterogenous translucent material description explained above and lighting conditions. The Stanford bunny model was used for it's complex 3D shape, comparable to real-life translucent objects, and it's familiarity and ability to be compared with future graphics work. All renders were created using the skylight-blue.tga light map which can be found in the freely available scenes from PBRT's authors.

5.6.2 Procedure

The perceived translucency of the heterogenous objects was established as a rating test. By simplifying the test to straight forward ratings, it allowed a coarse sorting of features that largely impacted the human perception of heterogenous materials. The users were asked to compare two images and mark which image appeared more translucent as can be seen in the sample test in figure 5.2. A comparison of two images was chosen in order to ensure that ratings could be analyzed without "tricking" the user into false translucency perception by manipulating factors such as scale that can impact the perception of translucency without providing valuable data for our study. The volunteers were asked to rate several image

pairs as to which appeared more translucent. All volunteers viewed the images on the same laptop and resolution. The image sets were randomized for each run and each volunteer rated each pair three times. No time limit was established for viewing each image, but participants were encouraged to go with their first reaction.

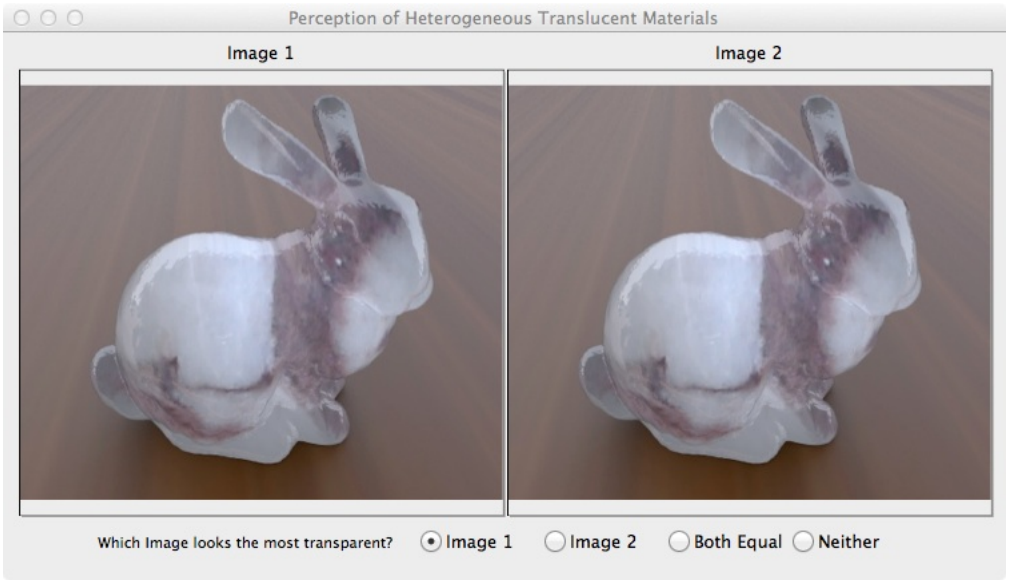

Figure 5.2: Perception Test Application

Chapter 6

Results and Discussion

6.1 Heterogeneous Translucent Material Description

6.1.1 Render Details

Images were created on a 3.06 GHz Intel Core 2 Duo Macbook Pro with 8 GB of 1067 MHz DDR3 and a NVIDIA GeForce 9600M GT 512 MB graphics card. The renders were all done at 640x480 pixels and a sampler rate of 32. The surface integrator was given a minsampledistance of .4 and a maxerror of .05. The primary light source for all renders is an infinite light source with 32 samples and an additional area light with 128 samples. Converting triangular surface meshes to tets was around a minute for single models using LibMesh. The libraries used for mesh creation and Finite Element solving are unfortunately not parallel implementations, but PBRT uses multiple cores when ever possible. The LibMesh library was also used for its matrix solver and mesh iteration functions.

Example Calculation Times

Model	Source Cost	Surface Cost	FE Assembly	Solution	Total
Bunny	19s	47s	11s	7s	84s

6.1.2 Material Parameters

The materials used for testing are based on parameters provided in Arbree's paper and are shown in Figure 6.1. Arbree arrived at the material models by orthographically projecting the images through the scattering geometry and determining the scattering coefficients from the returned pixel values [1]. The texture is rescaled to match the dynamic range of the scattering parameter using the range minimum and range maximum. By corresponding pixels in the scaled texture to a particular point, inverting it, and multiplying by the base scale, the scattering parameter is found. Since textures represent how much light is at each pixel, the texture needs to be inverted to represent how much light is lost during scattering [1]. For use in PBRT and for artist friendliness, my preferred method of specifying material properties is through the use of textures. For digital artists, textures provide a spacial layout of the material and it is easy to modify to reach a desired effect. σ_a is designed to take the full color texture for the absorption color, while σ'_s takes a greyscale version of the texture for the scatter color. This allows for easy placement and adjustment of heterogenous surfaces for artistic uses. A full example of the PBRT setup can be seen in Listing 6.1.

(a) (b) (c) (d) (e)

Model & Param.		Range Min	Range Max	Base Scale	Tex.
Dragon	σ_a	(.05, .05, .05)	(1.0, 1.0, 1.0)	(0.75, 1.25, 1.75)	(d)
Dragon	σ_s	(.25, .25, .25)	(1.0, 1.0, 1.0)	(16.7, 16.7, 16.7)	(e)
Geode	σ_a	(.01, .01, .01)	(1.0, 1.0, 1.0)	(5.0, 5.0, 5.0)	(c)
Geode	σ_s	constant	constant	(5.0, 5.0, 5.0)	–
Buddha	σ_a	constant	constant	(1.63, 1.18, 4.5)	–
Buddha	σ_s	(.05, .05, .05)	(1.0, 1.0, 1.0)	(16.7, 16.7, 16.7)	(a)
Bunny	σ_a	(.05, .05, .05)	(3.5, 3.5, 3.5)	(7.8, 7.8, 7.8)	(b)
Bunny	σ_s	(.60, .60, .60)	(1.0, 1.0, 1.0)	(13.1, 15.7, 18.0)	(b)

Figure 6.1: Parameters used to get realistic heterogeneous materials [1]

```
Film "image"
    "string filename" "marblebunnylightinginfinitefront36kr1.tga"

Sampler "lowdiscrepancy" "integer pixelsamples" [32]

LookAt 0 .2 .2    -.02 .1 0  0 1 0
Camera "perspective" "float fov" [60]

SurfaceIntegrator "dipolesubsurface" "float minsampledistance" [.4]
    "float maxerror" [.05]

WorldBegin

AttributeBegin
Rotate 90 1 0 0
LightSource "infinite" "integer nsamples" [32] # "color L" [1 1 1]
        "string mapname" ["/Users/lwieme/Desktop/pbrt-scenes/skylight-
           blue.tga"]

Material "matte" "color Kd" [0 0 0]

AreaLightSource "area" "color L" [4 4 4] "integer nsamples" [128]
Translate 0 10 0
Rotate 90 1 0 0
Shape "disk" "float radius" [8]

AttributeEnd

AttributeBegin
Translate 0 2 0
Rotate 90 1 0 0
AttributeEnd
Texture "oak" "color" "imagemap" "string filename" "/Users/lwieme/
   Desktop/pbrt-scenes/burloak.tga" "string mapping" "planar"

Material "plastic" "texture Kd" "oak" "color Ks" [.3 .3 .3]
Shape "trianglemesh" "point P" [ -1 0 -1 1 0 -1 1 0 1 -1 0 1 ]
  "integer indices" [ 0 1 2 2 3 0]

Texture "kd" "color" "imagemap" "string filename" "/Users/lwieme/Desktop
   /pbrt-scenes/marble2depth.tga" "string mapping" "planar" "float
   udelta" 1.3
  #"float uscale" 1 "float vscale" 1
Texture "mfp" "color" "imagemap" "string filename" "/Users/lwieme/
   Desktop/pbrt-scenes/marble2.tga" "string mapping" "planar" "float
   udelta" 1.3
  #"float uscale" 1 "float vscale" 1
Material "subsurface" "texture sigma_a" "mfp" #"texture meanfreepath" "
   mfp"
  "color Kr" [.1 .1 .1]
  "texture sigma_prime_s" "kd" "float scale" 3.6 #[.7 .0 .0]
```

```
Include "/Users/lwieme/Desktop/pbrt-scenes/geometry/bunny.pbrt"
WorldEnd
```

Listing 6.1: Example of Material Setup and Usage

6.1.3 Comparison to Previous Methods

Monte Carlo Methods

As discussed is section 4.1.1, Monte Carlo path tracing produces accurate renderings of heterogenous translucent materials and is able to reproduce highlights from non scattering caustic paths. This is currently a limitation of Finite Element solutions and such highlights are not included [1]. Also due to the basis projection used, the Finite Element solution is slightly more blurred than those produced with path tracing. However, Monte Carlo rendering is still extremely expensive. Artifact free images take considerably longer to achieve than comparable renders from the Finite Element solution.

Finite Difference Method

Before the Finite Element solution, Wang et al.'s iterative Finite Difference algorithm was considered the best approach for simulating heterogeneous scattering, while still heading towards a more generalized model [29]. Beginning with the diffusion equation, both the Finite difference Method and the Finite Element method have a similar level of inaccuracy due to approximation. The additional areas of error can be contributed to the FD algorithms utilization on PolyGrid mesh [8]. Notable differences from the Finite Element solution caused by the use of a PolyGrid include approximated boundary condition enforcement, the

distortion of the PolyGrid can be accurately modeled in the Finite Difference solution, and the grid loses nodes along boundary edges, creating error [1,8]. The Finite Element solution automatically generates the mesh without manual intervention, is faster to create, and lacks most or the error imposed on the Finite Difference method by the use of PolyGrids.

Previous FE Method

Adam Arbrees implementation of the Finite Element solution for modeling heterogeneous subsurface scattering materials set excellent ground work for an efficient and plausible model. Performance between his method and this method remain similar while achieving quality results. His work continued to focus on accurate reproduction, where the primary divergence of this work is to extend the range of perceptually believable materials that can easily be created and edited without being confined to measured data sets.

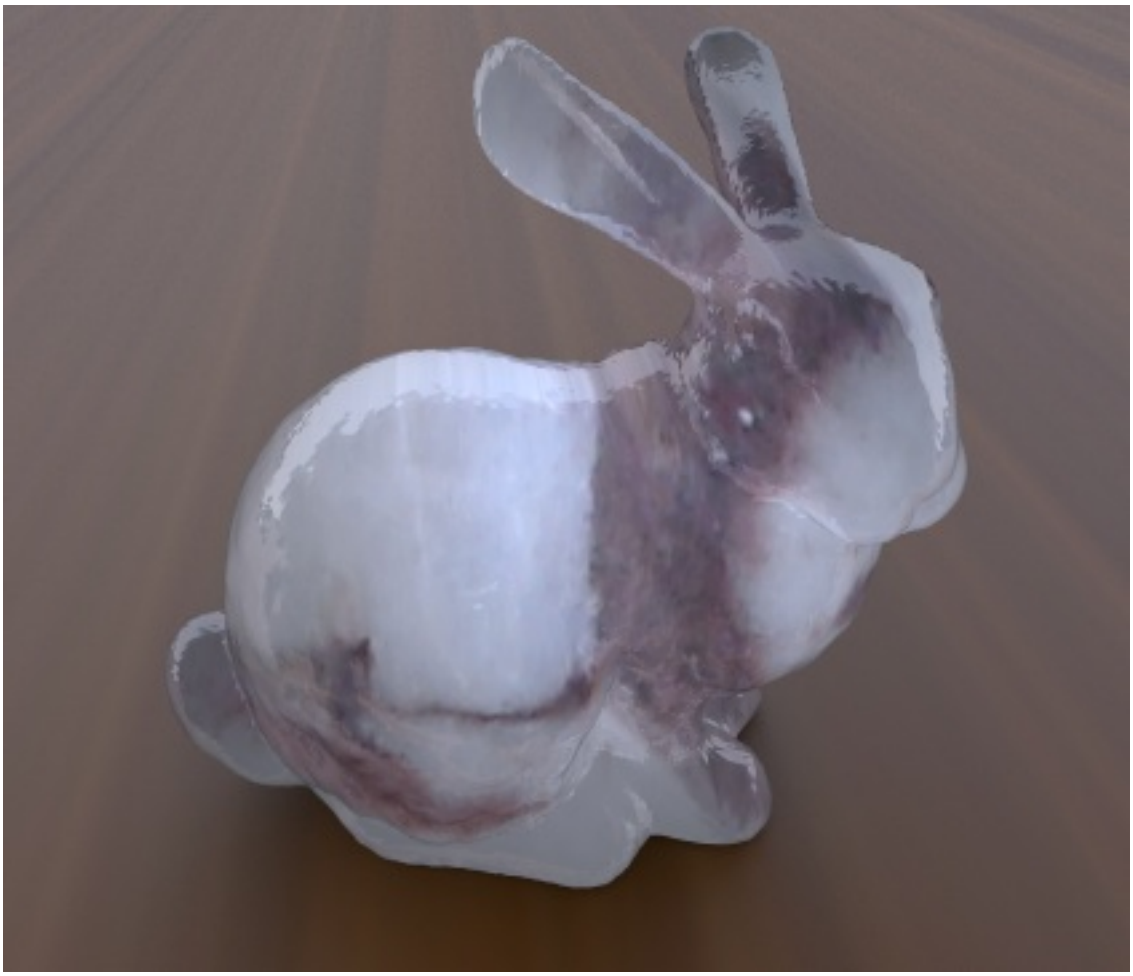

Figure 6.2: Results

6.2 Perception of Heterogeneous Translucent Materials

In section 5.6, the approach used for collecting data from human observers is documented. By studying the viewers reaction to changes to various factors, we can begin to generalize what characteristics the human visual system values in recognizing a translucent object. The factors of impact studied were illumination direction, color, contrast, blur, refractive index of the material, phase function, scattering coefficient, absorption coefficient, and specular highlights. Much of the work was found to be consistent with the work done

by Flemming et al. in Perceiving Translucent Materials [8], but there are some additional complexities to be studied with how we perceive a heterogeneous translucent material and why applying a homogeneous scattering solution breaks our perception of realism.

In previous work focused on homogeneous translucency, visual factors could be compared as changes over one unified object. The visual cues that trigger our perception of translucency remain the same across heterogeneously composed objects for each sub-material, but there is also an additional level of perception as we expect to note differences between each sub-material. For simplicity, a homogeneous scattering solution is frequently applied to a complex material such as granite. The human visual system sees this as a glaring break from reality as our eyes see what we know should be a conglomerate of materials, but they appear as though they are uniformly fused, receiving the same glow and highlights with no variation between sub-materials. In heterogenous materials, this establishes an importance for contrast between each visual factor of adjacent sub-materials. As Flemming found with lighting conditions and specular highlights [8], our perception is also forgiving of inconsistencies across sub-materials. Figures 6.3 and 6.4 show the impact of increasing Kr on viewers' perception of translucency. Flemming's test for the impact of lighting direction was repeated with heterogeneous material and the results are shown in figure 6.10. The impact of saturation was also recorded and documented for figure 6.5 and 6.6. With heterogeneous materials, we are looking for contrast and differences across the adjacent materials. As concluded from figure 6.6, exaggerating the contrast of visual cues between two adjacent sub-materials reinforces our perception that we are not looking at one uniform surface. It is because of this need to control contrast that image maps were chosen as the

input method for absorption and scattering. Examples of the textures used to alter contrast are shown in figure 6.8. These two parameters offer the most impact on the perception of translucency, other than appropriate lighting direction, and by using image maps, the areas of contrast are easily visualized and edited.

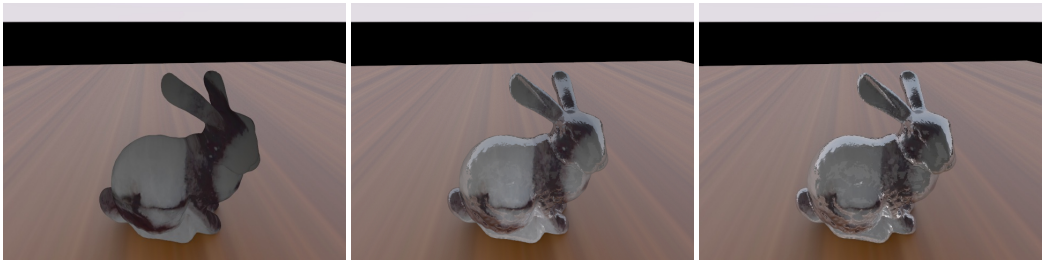

6.3a Kr of 0.0 6.3b Kr of 0.3 6.3c Kr of 0.5

Figure 6.3: Effects of Kr on the perception of heterogeneous translucency

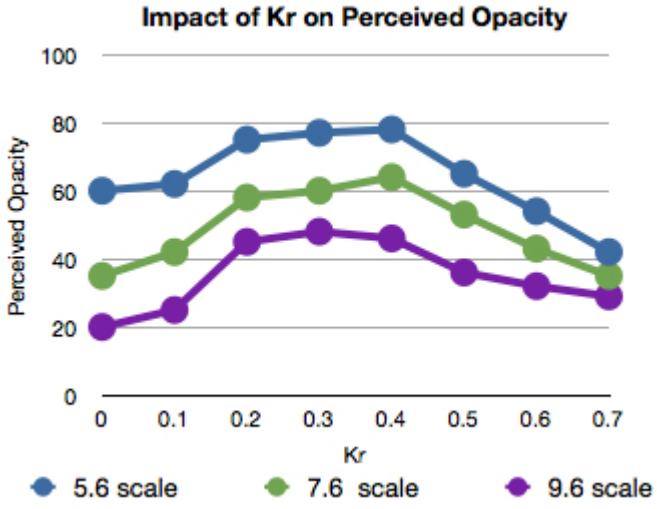

Figure 6.4: Kr was increased from 0.0 until renders became unreasonable shiny. The mean from 15 viewers was used graph the relationship between Kr values and the perceived heterogeneous translucency of renders done with 3 different scale values.

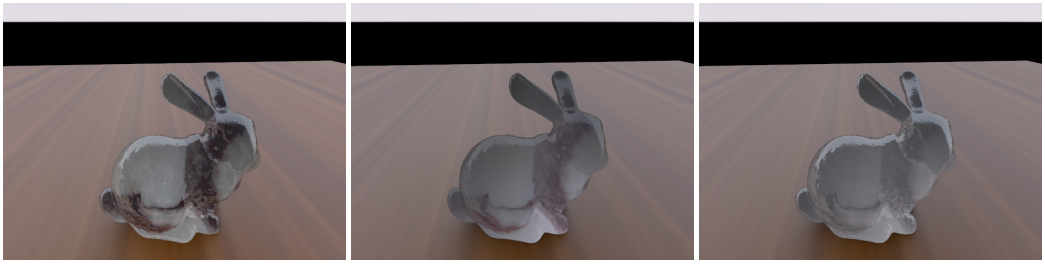

6.5a Saturated 6.5b Normal 6.5c Desaturated

Figure 6.5: Effects of saturation on the perception of heterogeneous translucency

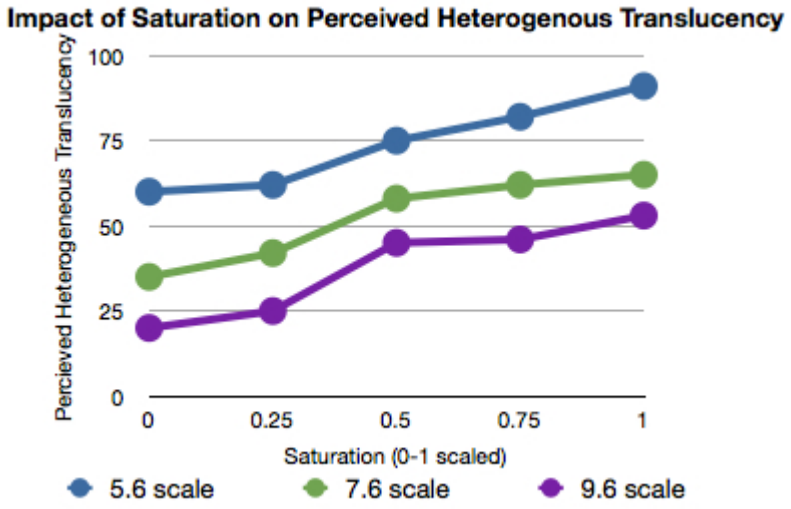

Figure 6.6: Saturation was increased from fully desaturated until renders became unreasonably saturated. The mean from 15 viewers was used graph the relationship between saturation values and the perceived heterogeneous translucency of renders done with 3 different scale values.

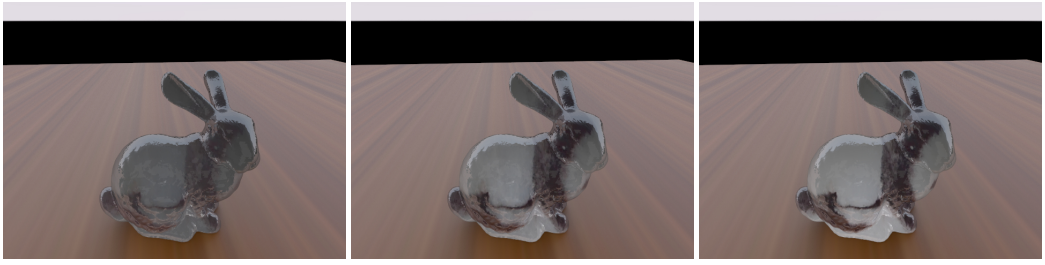

6.7a Less Contrast 6.7b Starting Contrast 6.7c More Contrast

Figure 6.7: Effects of contrast on the perception of heterogeneous translucency

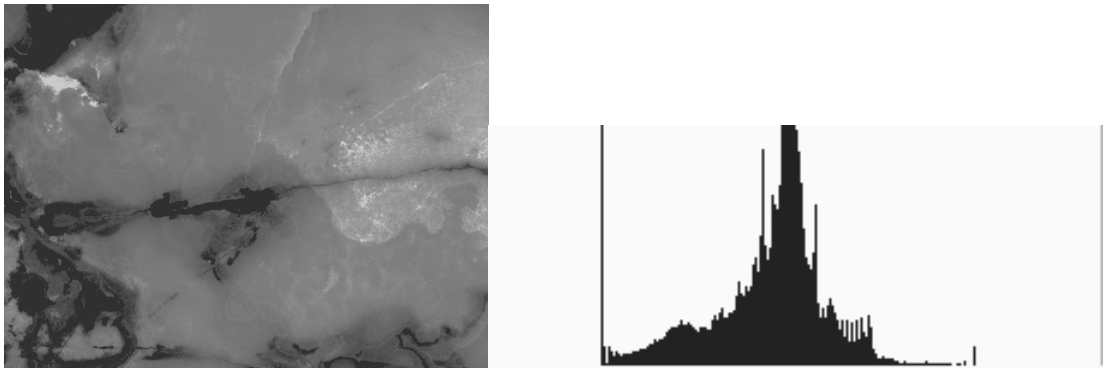

6.8a Less Contrast

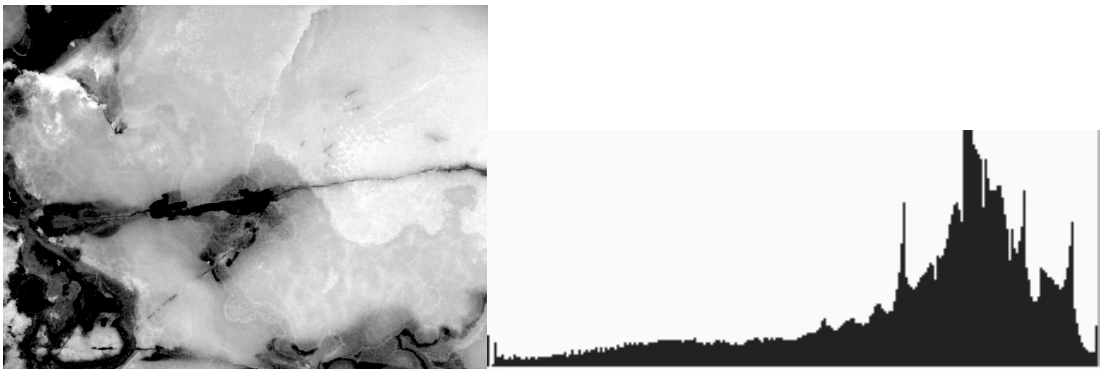

6.8b Starting Contrast

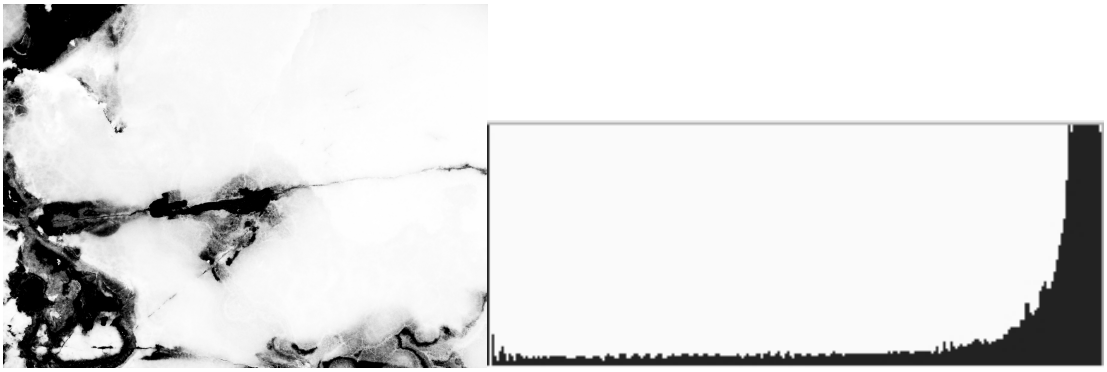

6.8c More Contrast

Figure 6.8: Adjustment to contrast of input textures

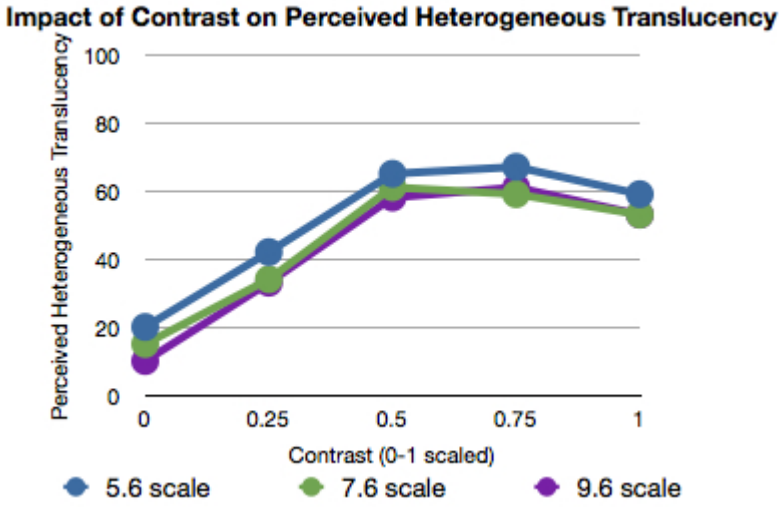

Figure 6.9: Contrast was increased from very low contrast to very high contrast. The mean from 15 viewers was used graph the relationship between contrast values and the perceived heterogeneous translucency of renders done with 3 different scale values.

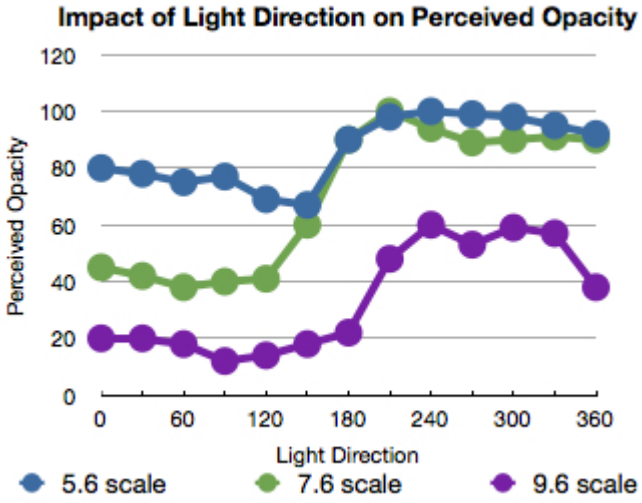

Figure 6.10: Lighting was rotated around the object to gauge the effect of light direction on the perceived heterogeneous translucency. The object was lit from behind when the angle was less than 180 degrees and light from the front when angles were greater than 180 degrees. The mean from 15 viewers was used graph the relationship between light direction values and the perceived heterogeneous translucency of renders done with 3 different scale values.

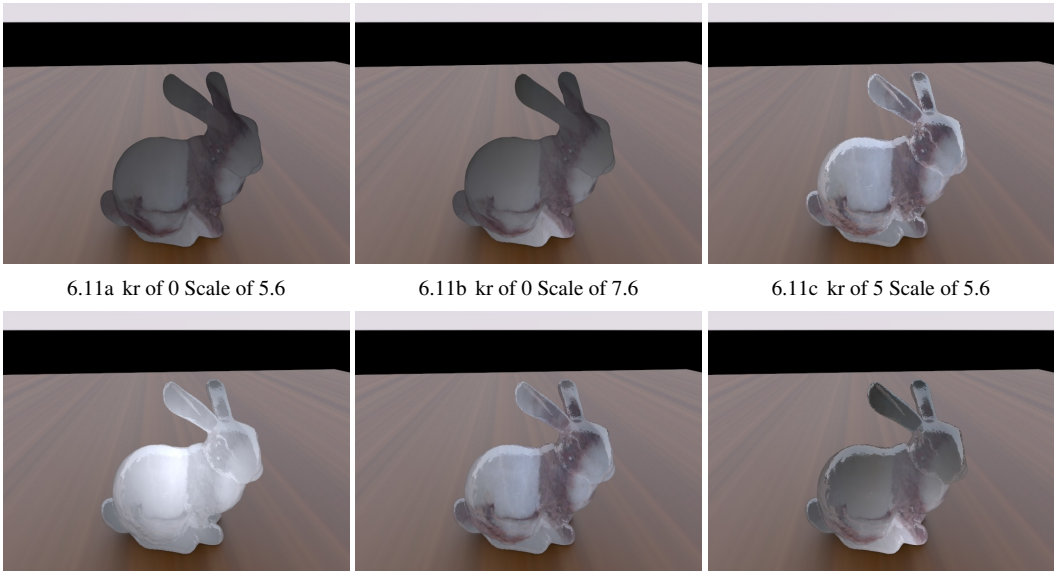

6.11a kr of 0 Scale of 5.6 | 6.11b kr of 0 Scale of 7.6 | 6.11c kr of 5 Scale of 5.6

6.11d Desaturated | 6.11e Scale of 5.6 | 6.11f Scale of 9.6

Figure 6.11: Additional samples of render variations

Chapter 7

Conclusion

This work advances heterogenous translucent material models to a wider audience, allowing computer graphics artists to simulate a larger range of surfaces. The documented approach to heterogeneous subsurface scattering creates a more generalized material description and benefits from perception testing to maintain a reasonable approximation of translucency. The work leverages the strengths of Finite Element Systems to simplify the scattering in heterogenous materials while providing quality renders and an easily modifiable material description. The method was validated by creating a set of test renders and allowing a group of volunteers to evaluate the perceived translucency of the resultant images.

Chapter 8

Future Work

Due to the shear scale of the problem of heterogeneous subsurface scattering and how current the topic is, there is plenty of future work that could be done. The material description in this work is based off of the diffusion approximation. The diffusion approximation is a familiar algorithm and was suitably efficient for this paper's intended use in film rendering; however, the diffusion approximation is a simplified scattering model and work could be done to improve areas of inaccuracy, especially as hardware continues to improve. Also, I found working in PBRT to be restrictive and many of the math libraries used for Finite Element solutions are out dated. Future work may benefit from a C++ plugin approach, suitable for use in various rendering packages, and ideally a new library could be created with solving rendering problems in mind. Finally, PBRT and the algorithms used in this paper are using primarily software for computation. The computations required to render heterogeneous translucent materials, particularly using the Finite Element solution, could benefit from use of the GPU.

Bibliography

[1] Adam Arbree, Bruce Walter, and Kavita Bala. Diffusion formulation for heterogeneous subsurface scattering. 2009.

[2] Adam Arbree, Bruce Walter, and Kavita Bala. Heterogeneous Subsurface Scattering Using the Finite Element Method. *IEEE Transactions on Visualization and Computer Graphics*, 17(7), July 2011.

[3] Christian Boucheny, Georges-Pierre Bonneau, Jacques Droulez, Guillaume Thibault, and Stephane Ploix. A perceptive evaluation of volume rendering techniques. *Transactions on Applied Perception (TAP*, 5(4), January 2009.

[4] Subrahmanyan Chandrasekhar. *Radiative transfer*. Courier Dover Publications, 1960.

[5] C Delalandre, P Gautron, J E Marvie, and G François. Single scattering in heterogenous participating media. *ACM SIGGRAPH 2010 Talks*, page 14, 2010.

[6] Cyril Delalandre, Pascal Gautron, Jean-Eudes Marvie, and Guillaume Fran c c ois. Single scattering in heterogenous participating media. *International Conference on Computer Graphics and Interactive Techniques*, 2010.

[7] Craig Donner, Jason Lawrence, Ravi Ramamoorthi, Toshiya Hachisuka, Henrik Wann

Jensen, and Shree Nayar. An empirical BSSRDF model. *ACM Transactions on Graphics*, 28(3):1, 2009.

[8] R W Fleming, H W Jensen, and H H Bulthoff. Perceiving translucent materials. *ACM International . . .*, 2004.

[9] Roland W Fleming and Heinrich H B u lthoff. Low-Level Image Cues in the Perception of Translucent Materials. *ACM Transactions on Applied Perception (TAP)*, 2(3):346, 2005.

[10] Christian Fuchs, Michael Goesele, Tongbo Chen, and Hans-Peter Seidel. An empirical model for heterogeneous translucent objects. *International Conference on Computer Graphics and Interactive Techniques*, 2005.

[11] Michael Goesele, Hendrik P A Lensch, Jochen Lang, Christian Fuchs, and Hans-Peter Seidel. DISCO: acquisition of translucent objects. *International Conference on Computer Graphics and Interactive Techniques*, 23(3):835, 2004.

[12] Tom Haber, Tom Mertens, Philippe Bekaert, and Frank Van Reeth. A computational approach to simulate subsurface light diffusion in arbitrarily shaped objects. *ACM International Conference Proceeding Series; Vol. 112*, page 79, 2005.

[13] Pat Hanrahan and Wolfgang Krueger. Reflection from layered surfaces due to subsurface scattering. *International Conference on Computer Graphics and Interactive Techniques*, page 165, 1993.

[14] M Hašan, M Fuchs, W Matusik, H Pfister, and S Rusinkiewicz. Physical reproduction

of materials with specified subsurface scattering. *ACM Transactions on Graphics (TOG)*, 29(4):61, 2010.

[15] A Ishimaru. Forward scatter theory and diffusion theory for waves in random media. In *Antennas and Propagation Society International Symposium, 1979*, pages 16–16, 1979.

[16] Wojciech Jarosz. Efficient Methods for General Light Transport Simulation in Scattering Media. pages 1–220, August 2011.

[17] H W Jensen, S R Marschner, M Levoy, and P Hanrahan. A practical model for subsurface light transport. *Proceedings of the 28th annual conference on Computer graphics and interactive techniques*, pages 511–518, 2001.

[18] Henrik Wann Jensen and Juan Buhler. A rapid hierarchical rendering technique for translucent materials. *ACM Transactions on Graphics (TOG)*, 21(3):576, 2002.

[19] Henrik Wann Jensen and Per H Christensen. Efficient simulation of light transport in scences with participating media using photon maps. *International Conference on Computer Graphics and Interactive Techniques*, page 311, 1998.

[20] Henrik Wann Jensen, Justin Legakis, Julie Dorsey, Jensen Justin, and Legakis Julie Dorsey. Rendering of Wet Materials. Technical report, 1999.

[21] I Motoyoshi. Highlight-shading relationship as a cue for the perception of translucent and transparent materials. *Journal of Vision*, 10(9):6–6, July 2010.

[22] Mark Pauly, Thomas Kollig, and Alexander Keller. Metropolis Light Transport for

Participating Media. *Proceedings of the Eurographics Workshop on Rendering Techniques 2000*, page 11, 2000.

[23] Pieter Peers, Karl vom Berge, Wojciech Matusik, Ravi Ramamoorthi, Jason Lawrence, Szymon Rusinkiewicz, and Philip Dutr e. A compact factored representation of heterogeneous subsurface scattering. *ACM SIGGRAPH 2006 Papers on - SIGGRAPH '06*, page 746, 2006.

[24] Matt Pharr and Greg Humphreys. Physically Based Rendering: From Theory to Implementation. 2010.

[25] Holly Rushmeier. The perception of simulated materials. *International Conference on Computer Graphics and Interactive Techniques*, 2008.

[26] Ying Song, Xin Tong, Fabio Pellacini, and Pieter Peers. SubEdit : A Representation for Editing Measured Heterogeneous Subsurface Scattering. 2006.

[27] Sarah Tariq, Andrew Gardner, Ignacio Llamas, Andrew Jones, Paul Debevec, and Greg Turk. Efficient Estimation of Spatially Varying Subsurface Scattering Parameters.

[28] X Tong, J Wang, S Lin, B Guo, and H Y Shum. Modeling and rendering of quasi-homogeneous materials. *ACM Transactions on Graphics (TOG)*, 24(3):1054–1061, 2005.

[29] Jiaping Wang, Shuang Zhao, Xin Tong, Stephen Lin, Zhouchen Lin, Yue Dong, Baining Guo, and Heung-Yeung Shum. Modeling and rendering of heterogeneous translucent materials using the diffusion equation. *ACM Transactions on Graphics*, 27(1):1–18, March 2008.

[30] Jiaping Wang, Shuang Zhao, Xin Tong, Stephen Lin, Zhouchen Lin, Yue Dong, Baining Guo, and Heung-Yeung Shum. Modeling and rendering of heterogeneous translucent materials using the diffusion equation. *ACM Transactions on Graphics (TOG)*, 27(1), 2008.